Efficient band-pass color filters enabled by resonant modes and plasmons near the Rayleigh anomaly

Daniel B. Mazulquim,[1,2] Kyu Jin Lee,[1] Jae Woong Yoon,[1] Leone V. Muniz,[2] Ben-Hur V. Borges,[2] Luiz G. Neto,[2] and Robert Magnusson[1,*]

[1]*Department of Electrical Engineering, University of Texas - Arlington, Box 19016, Arlington, Texas 76019, USA*
[2]*Department of Electrical Engineering, EESC, University of São Paulo, 13566-590 São Carlos, Brazil*
[*]*magnusson@uta.edu*

Abstract: We design and fabricate efficient, narrow-band, transmission color filters whose operating principle resides in a narrow-band guided-mode resonance associated with a surface-plasmon resonance. The fundamental device consists of an aluminum grating over a 200-nm-thick aluminum oxide film on a glass substrate. Numerical simulations show a sharp resonance-derived spectral profile that is additionally shaped by a neighboring Rayleigh anomaly. Besides the Rayleigh effect, we show numerically that the narrow bandwidth is predominantly due to the low refractive-index contrast between the waveguide film and the substrate. Red, green, and blue filters are fabricated using ultraviolet holographic lithography followed by a lift-off process. The experimental spectral efficiency in transmission exceeds 80% with full-width-at-half-maximum linewidths near 20 nm. We provide color images of the zero-order transmitted spectra, and illustrate the pure colors associated with the modal resonance extracted as side-coupled output light.

OCIS codes: (130.7408) Wavelength filtering devices; (050.1950) Diffraction gratings; (230.5750) Resonators; (310.6628) Subwavelength structures, nanostructures.

References and links

1. R. W. Sabnis, "Color filter technology for liquid crystal display," Displays **20**(3), 119–129 (1999).
2. Yan Yu, L. Wen, S. Song, and Q. Chen, "Transmissive/Reflective Structural Color Filters: Theory and Applications," J. Nano Mat. 212637 (2014).
3. H. S. Lee, Y. T. Yoon, S. S. Lee, S. H. Kim, and K. D. Lee, "Color filter based on a subwavelength patterned metal grating," Opt. Express **15**(23), 15457–15463 (2007).
4. Q. Chen and D. R. S. Cumming, "High transmission and low color cross-talk plasmonic color filters using triangular-lattice hole arrays in aluminum films," Opt. Express **18**(13), 14056–14062 (2010).
5. G. Si, Y. Zhao, H. Liu, S. Teo, M. Zhang, T. J. Huang, A. J. Danner, and J. Teng, "Annular aperture array based color filter," Appl. Phys. Lett. **99**(3), 033105 (2011).
6. S. Yokogawa, S. P. Burgos, and H. A. Atwater, "Plasmonic color filters for CMOS image sensor applications," Nano Lett. **12**(8), 4349–4354 (2012).
7. R. Girard-Desprolet, S. Boutami, S. Lhostis, and G. Vitrant, "Angular and polarization properties of cross-holes nanostructured metallic filters," Opt. Express **21**(24), 29412–29424 (2013).
8. Y. T. Yoon and S. S. Lee, "Transmission type color filter incorporating a silver film based etalon," Opt. Express **18**(5), 5344–5349 (2010).
9. V. R. Shrestha, S. S. Lee, E. S. Kim, and D. Y. Choi, "Non-iridescent transmissive structural color filter featuring highly efficient transmission and high excitation purity," Sci Rep **4**, 4921 (2014).
10. K. T. Lee, S. Seo, J. Y. Lee, and L. J. Guo, "Ultrathin metal-semiconductor-metal resonator for angle invariant visible band transmission filters," Appl. Phys. Lett. **104**(23), 231112 (2014).
11. M. J. Uddin and R. Magnusson, "Efficient guided-mode resonant tunable color filter," IEEE Photon. Technol. Lett. **24**(17), 1552–1554 (2012).
12. M. J. Uddin and R. Magnusson, "Highly efficient color filter array using resonant Si3N4 gratings," Opt. Express **21**(10), 12495–12506 (2013).
13. M. J. Uddin, T. Khaleque, and R. Magnusson, "Guided-mode resonant polarization-controlled tunable color filters," Opt. Express **22**(10), 12307–12315 (2014).
14. Y. T. Yoon, C. H. Park, and S. S. Lee, "Highly efficient color filter incorporating a thin metal-dielectric resonant structure," Appl. Phys. Express **5**(2), 022501 (2012).

#223907 - $15.00 USD Received 26 Sep 2014; revised 19 Nov 2014; accepted 25 Nov 2014; published 4 Dec 2014

15. A. F. Kaplan, T. Xu, and L. J. Guo, "High efficiency resonance-based spectrum filters with tunable transmission bandwith fabricated using nanoimprint lithography," Appl. Phys. Lett. **99**(14), 143111 (2011).
16. C. H. Park, Y. T. Yoon, and S. S. Lee, "Polarization-independent visible wavelength filter incorporating a symmetric metal-dielectric resonant structure," Opt. Express **20**(21), 23769–23777 (2012).
17. C. H. Park, Y. T. Yoon, V. R. Shrestha, C. S. Park, S. S. Lee, and E. S. Kim, "Electrically tunable color filter based on a polarization-tailored nano-photonic dichroic resonator featuring an asymmetric subwavelength grating," Opt. Express **21**(23), 28783–28793 (2013).
18. V. R. Shrestha, C. S. Park, and S. S. Lee, "Enhancement of color saturation and color gamut enabled by a dual-band color filter exhibiting an adjustable spectral response," Opt. Express **22**(3), 3691–3704 (2014).
19. www.comsol.com.
20. D. Y. Smith, E. Shiles, and M. Inokuti, "The optical properties of metallic aluminum," E. D. Palik ed., in *Handbook of Optical Constants of Solids* (Academic Press 1998).
21. M. S. Amin, J. W. Yoon, and R. Magnusson, "Optical transmission filters with coexisting guided-mode resonance and Rayleigh anomaly," Appl. Phys. Lett. **103**(13), 131106 (2013).

1. Introduction

Transmission color filters are widely used in imaging cameras, computer monitors, and projection display systems. Intrinsic heating and low color selectivity hamper conventional color filters made with liquid crystals and dye molecules [1]. Color filters fashioned with photonic nanostructures possess advantages over dye-based filters in tunability, compactness, stability, and multi-functionality [2]. Recently, many types of thin-film color filters have been suggested using surface-plasmonic crystals [3–7], Fabry-Pérot resonators [8–10], and guided-mode resonant subwavelength gratings [11–14]. In particular, guided-mode resonance (GMR) filters with metal films are presently attracting special attention. In this device class, a structure with metallic gratings and two dielectric layers for waveguide and buffer cladding has shown promising performance [15–18]. Another architecture incorporating a single dielectric layer underneath metallic gratings was suggested in this context, but its performance is limited with relatively large transmission bandwidth [14,15]. For practical applications, it is desirable to reduce the number of fabrication steps while maintaining high performance.

In this paper, we present comprehensive theoretical and experimental analyses of metallic GMR color filters incorporating a single dielectric waveguide layer. The filter operates with cooperating guided-mode and surface-plasmon resonance effects near the Rayleigh anomaly wavelength. We numerically show that the narrow transmission bandwidth obtained is primarily due to a low contrast in the index of refraction between the waveguide core and the substrate. Using a standard lift-off process with laser interference lithography appropriate for economical large-area nanopatterning, we fabricate the optimized design with a subwavelength Al grating on Al_2O_3 waveguide layer. We experimentally demonstrate high peak efficiency exceeding 80% and superb color purity provided by associated narrow bandwidths of ~20 nm for the three fundamental colors at 454 nm, 536 nm, and 651 nm wavelengths.

2. Design

Our basic device consists of an Al_2O_3 waveguide layer between a glass substrate and a periodic array of Al slits on top, as illustrated in Fig. 1. The geometric parameters to be optimized are the grating period Λ, grating fill factor F, grating thickness t_g, and the waveguide thickness t_f. We use the finite element method (FEM) [19] for the numerical calculations. The FEM method with adaptive triangular meshes is highly appropriate for numerical calculation of metallic nanostructures that demand deep subwavelength spatial discretization to properly describe quickly decaying fields near the metal surfaces. To analyze the optical response of the color filters, we calculate the transmittance spectrum in the visible regime (400–750 nm) for blue, green and red filters, varying the Al_2O_3 film thickness from 0 to 400 nm. We use realistic optical constants of Al, listed in [20] and Al_2O_3, obtained by our own ellipsometric measurements, as shown in Fig. 1(b). The refractive index of the glass substrate is constant at 1.518 in the numerical calculations. We assume an incident plane wave with transverse magnetic (TM) polarization, with its magnetic field oscillating along the grating ridges and the electric fields oscillating in the plane of incidence, as noted in Fig. 1(a).

#223907 - $15.00 USD Received 26 Sep 2014; revised 19 Nov 2014; accepted 25 Nov 2014; published 4 Dec 2014

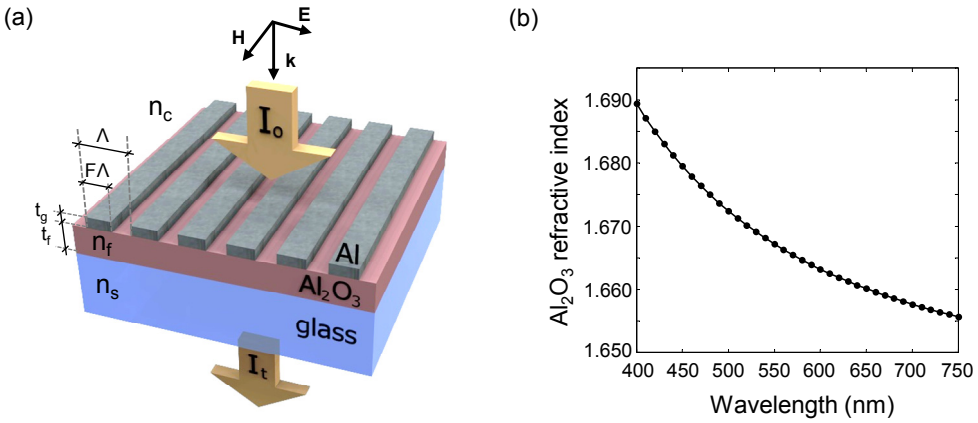

Fig. 1. (a) Schematic of a color filter incorporating coexisting GMR and SPR effects. The parameters n_s, n_f, and n_c denote refractive indices of glass substrate, Al_2O_3 film, and air cover, respectively. For geometrical parameters, Λ is the period, F is the fill factor and t_g and t_f are the thicknesses of Al gratings and Al_2O_3 film, respectively. I_0 and I_t indicate the intensity of the incident and transmitted light waves, respectively. (b) Al_2O_3 refractive index data measured by ellipsometry.

A parametric search based on trial solutions yields t_g = 40 nm, F = 0.67 and Λ = 290 nm, 350 nm, and 430 nm for blue, green, and red filters, respectively. The calculated transmission spectra with varying Al_2O_3 thickness t_f are shown in Fig. 2. As the Al_2O_3-thickness-dependent transmittance spectra illustrate, there appear no transmission peaks without the Al_2O_3 film (t_f = 0). A narrow transmission peak and fairly low sidebands emerge with increasing film thickness as the Al_2O_3 layer admits the fundamental guided mode. Considering practical devices with three fundamental color filters integrated in a single panel, it is desirable to obtain high spectral performance for the three color filter elements at the identical film thicknesses. In our design, the three color filters have desired spectral properties around t_f = 200 nm as shown in Figs. 2(d)–2(f). At t_f = 200 nm, the efficiency of all three filters approaches 90%. The full-width at half maximum (FWHM) peak efficiency is 22 nm centered at wavelength 456 nm for the blue filter; 20 nm centered at wavelength 541 nm for the green filter; and 14 nm centered at wavelength 655 nm for the red filter.

A narrow-band guided-mode resonance coupled with a surface-plasmon resonance (SPR) forms the obtained spectral profile. The leaky mode induces the transmission peak at the phase matching condition $k_{||} = \beta \pm 2\pi q/\Lambda$, where $k_{||}$ is the in-plane wavevector of the incident light, β is the propagation constant of the guided mode, and q is the diffraction-order index. Inset I of Fig. 2(d) shows the magnetic field distribution at the transmission peak wavelength. It shows a predominant field pattern of a TM_0 guided mode in this metal-coupled dielectric waveguide; local plasmonic fields generated at the Al grating ridges as shown affect the mode shape. The field distribution for the transmission minimum wavelength is shown in inset II of Fig. 2(d). We confirm a typical surface plasmonic field pattern excited on the Al-Al_2O_3 interface. Note that the absolute values of the magnetic fields in these patterns are self-normalized by their maximum values for improved visualization.

#223907 - $15.00 USD Received 26 Sep 2014; revised 19 Nov 2014; accepted 25 Nov 2014; published 4 Dec 2014

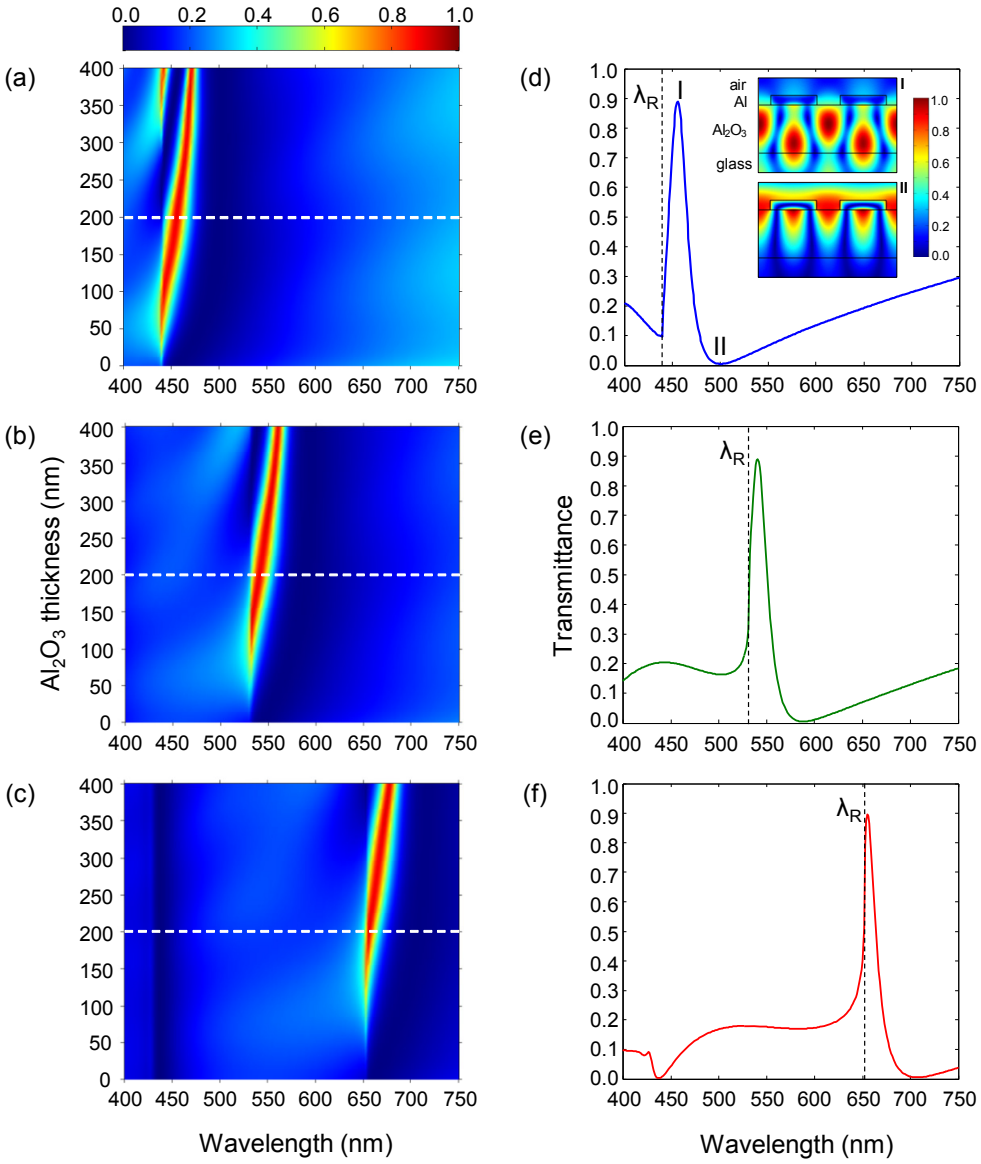

Fig. 2. Theoretical performance of our color filters. Al_2O_3-film-thickness-dependent transmittance spectra for (a) blue (Λ = 290 nm), (b) green (Λ = 350 nm), and (c) red (Λ = 430 nm) filters. Fixed parameters are t_g = 40 nm and F = 0.67. Spectral profiles of the transmittance at fixed Al_2O_3 film thickness (t_f = 200 nm) for (d) blue (Λ = 290 nm), (e) green (Λ = 350 nm), and (f) red (Λ = 430 nm) filters. Insets I and II in (d) show the magnetic field amplitude |(**H**)| for the peak wavelength (I) and transmission minimum (II), respectively. Note that the field amplitudes are self-normalized by their maximum values in both insets. The vertical dashed lines in (d)~(f) indicate the Rayleigh anomaly wavelengths.

Interestingly, Figs. 2(a)–2(c) show that the transmission peak becomes remarkably narrower for the Al_2O_3 film thickness ranges of 50 nm < t_f < 150 nm in Fig. 2(a), 100 nm < t_f < 200 nm in Fig. 2(b), and 150 nm < t_f < 250 nm in Fig. 2(c). This is understood by a neighboring Rayleigh anomaly affecting the modal resonance spectrum. For a non-metallic resonance device, it was shown that the onset of higher diffraction orders at the Rayleigh anomaly can sharpen a resonance-induced transmission peak in both spectral and angular domains [21]. Here, a similar zero-order wave suppression results in rapid decrease of the

#223907 - $15.00 USD Received 26 Sep 2014; revised 19 Nov 2014; accepted 25 Nov 2014; published 4 Dec 2014

filter efficiency in the shorter wavelength vicinity of the Rayleigh anomaly and forms a sharper spectral profile. This effect involves resonantly enhanced fields and associated optical power leakage along the direction tangential to the device surface [20]. In our case, the Rayleigh anomaly is located at wavelengths $\lambda_R = n_s\Lambda = 440$ nm in Fig. 2(a), 531 nm in Fig. 2(b), and 653 nm in Fig. 2(c), where n_s denotes refractive index (1.518 in our case) of the substrate. The vertical dashed lines in Figs. 2(d)–2(f) indicate the Rayleigh anomaly wavelengths. The separations between λ_R and the resonance peak wavelengths are 16, 10, and 2 nm, for blue, green, and red filters, respectively.

Besides the effect of the Rayleigh anomaly, the narrow transmission bandwidth in our design is due to low index-contrast between the waveguide core and the substrate. Figure 3 shows the calculated spectral response of the blue filter with varying film thickness. We consider three different refractive indices of the waveguide layer $n_f \in \{2.5, 2.0, 1.7\}$. A noticeable decrease of the transmission bandwidth with decreasing n_f is seen. A low index-contrast between the waveguide film and the substrate leads to larger mode field diameter and relatively smaller portion of the confined energy at the metal grating layer. These factors reduce the ohmic absorption and radiation damping of the guided mode, resulting in a narrowed bandwidth.

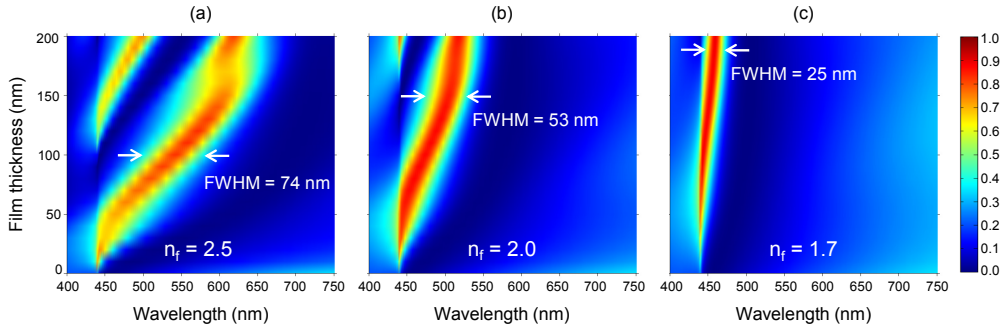

Fig. 3. Calculated spectral response of the blue filter considering three different refractive indices of the film (a) $n_f = 2.5$, (b) $n_f = 2.0$, and (c) $n_f = 1.7$. Representative values of the FWHM are shown at (a) $t_f = 100$ nm, (b) $t_f = 150$ nm, and (c) $t_f = 190$ nm. Fixed parameters are $\Lambda = 290$ nm, $F = 0.67$, $t_g = 40$ nm, and $n_s = 1.518$.

In addition, Fig. 2 shows that the calculated spectra are fairly tolerant against the Al_2O_3-film thickness variation. There is a region near $t_f = 200$ nm for the three filters where they present acceptable performance. The resonant wavelength can be directly tuned by the grating period. We note that corresponding polarization-independent filters can be readily obtained by producing a 2D analogy of our 1D array design.

The filters are designed to work at normal incidence. To estimate their angular aperture, we calculate the transmission spectrum considering a range of ± 10° from normal incidence. At the peak wavelengths, the FWHM for the blue, green and red filters are 5.2°, 4.2°, and 3.4°, respectively. These values correspond to the angular ranges in which the transmission is equal to or above 50% of the maximum transmission at normal incidence. Therefore, the filters will provide acceptable performance under collimated beam incidence with divergence angle within the respective angular bandwidth.

3. Fabrication and characterization

We fabricate the designed color filters with standard nanolithography processes. Initially, we deposit a 200-nm-thick Al_2O_3 film on a glass substrate using ultrahigh vacuum radio-frequency sputtering system (AJA ETC Orion series). The film thickness and refractive index are measured using ellipsometry (VB-400, VASE ellipsometer system, J. A. Woollam). Next a 240-nm-thick positive photoresist (PR) is spin-coated at 3000 rpm over the Al_2O_3 film. The sample is then pre-baked for 90 seconds at 110 °C. To produce the one-dimensional gratings,

#223907 - $15.00 USD Received 26 Sep 2014; revised 19 Nov 2014; accepted 25 Nov 2014; published 4 Dec 2014

we use an ultraviolet laser holographic lithography system operating at the 266 nm wavelength. Then a 40-nm-thick Al film is sputtered on the photoresist patterned 1D grating. Finally, we use a lift-off process to establish a top Al grating layer. Figure 4 summarizes the fabrication process.

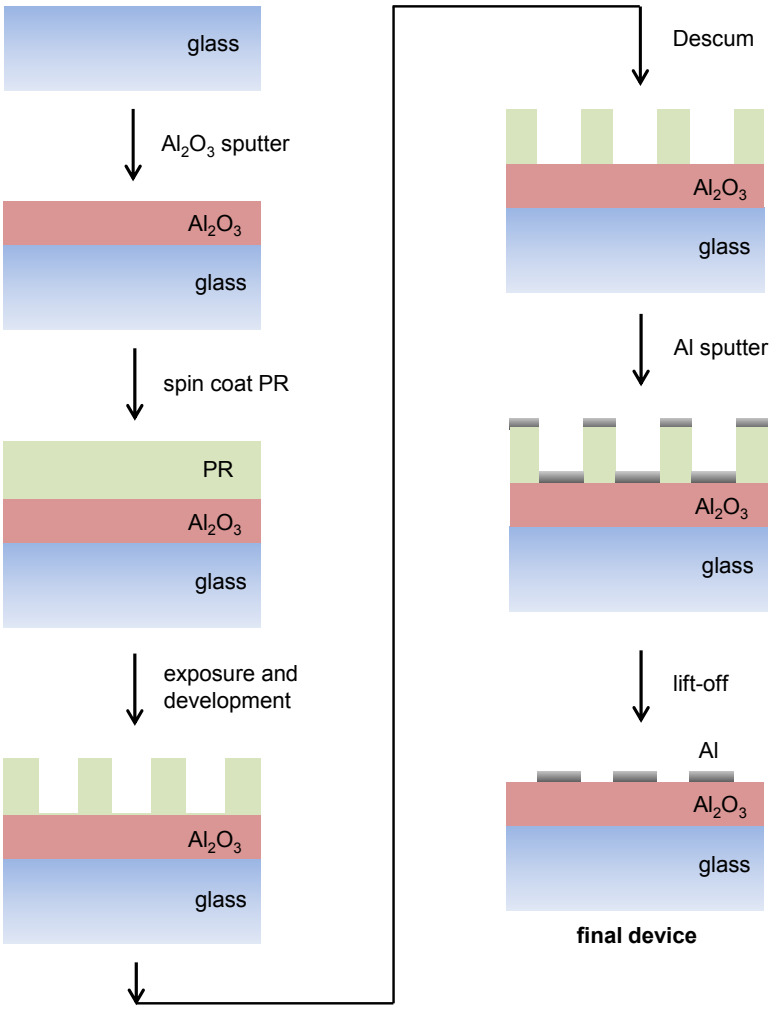

Fig. 4. Fabrication process flow.

The fabricated Al_2O_3 film thicknesses are 203 nm, 203 nm and 208 nm for the blue, green, and red filters, respectively. We measure the obtained device parameters such as period, fill factor, and grating height using atomic force microscopy (AFM). The AFM images and profiles are shown in Fig. 5. The measured parameters are: $\Lambda \approx 291$ nm, $F \approx 0.656$, and $t_g \approx 40$ nm for the blue filter; $\Lambda \approx 349$ nm, $F \approx 0.665$, and $t_g \approx 40$ nm for the green filter; and $\Lambda \approx 428$ nm, $F \approx 0.678$, and $t_g \approx 38$ nm for the red filter. Measurement error ranges are estimated as ± 1.3 nm for Λ, ± 0.003 for F, and ± 3.3 nm for t_g. In each case, the measured parameters are reasonably close to those of the design.

#223907 - $15.00 USD Received 26 Sep 2014; revised 19 Nov 2014; accepted 25 Nov 2014; published 4 Dec 2014

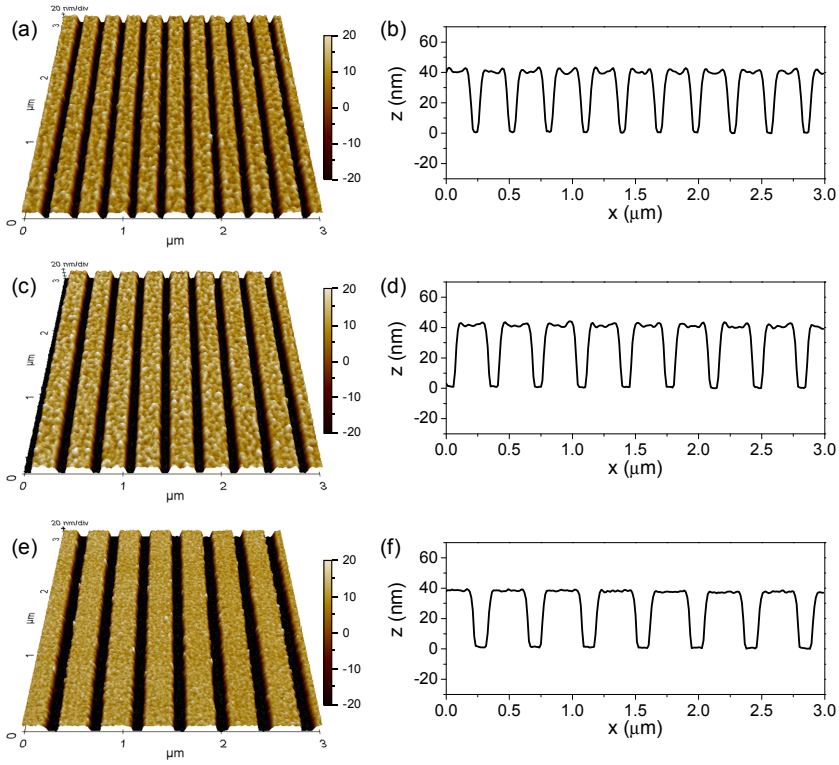

Fig. 5. AFM images and profiles of the fabricated (a,b) blue, (c,d) green, and (e,f) red filters.

4. Results and discussion

We measure the spectral response of the fabricated color filters using an optical spectrum analyzer (Ocean Optics USB4000). We use a tungsten halogen lamp covering the wavelength range from 360 to 2400 nm (Ocean Optics HL-2000) as a light source. Collimated white light passes through a linear polarizer for TM-polarized light incidence on the sample. A fiber optic cable transmitting the signal to the spectrum analyzer then collects the transmitted light. We obtain the absolute transmittance spectrum by normalizing the signal with the spectral power density of the light source. In the signal normalization, we take a 4.2% reflection on the bottom surface of the glass substrate into account.

The spectral results are shown in Figs. 6(a)–6(c). The experimental spectra for all the three filters quantitatively agree with the simulation using the fabricated parameters. Each fabricated color filter presents high efficiency with narrow transmission peak. The efficiency is 81%, 82%, and 80% for the blue, green, and red filters, respectively. Measured FWHM of the peaks are 19 nm centered at 454 nm for the blue filter; 20 nm centered at 536 nm for the green filter; and 19 nm centered at 651 nm for the red filter. Figures 6(d)–6(f) show color images of the zero-order transmission (T_0) observed for the blue, green, and red filters. Since our white light source has a band concentrated in the red region – the intensity at 650 nm is around 9 times larger than at 450 nm – we note a "purpled" color for the zero-order transmission of the blue filter in Fig. 6(d). The "orange" color observed for the red filter in Fig. 6(f) is associated with the significant measured side band of the device. The perceived colors of the zero-order transmission can be tailored to some degree since they depend on the shape of the white-light source spectrum. Besides the zero-order transmission images – in which the devices are designed to work – we are able to obtain the guided-mode images also. Figures 6(g)–6(i) show the observed side-coupled beams, which propagate in the

#223907 - $15.00 USD Received 26 Sep 2014; revised 19 Nov 2014; accepted 25 Nov 2014; published 4 Dec 2014

homogeneous film leaving the device in a direction perpendicular to the incident beam. We observe high-purity blue, green, and red colors associated with the guided-mode resonance.

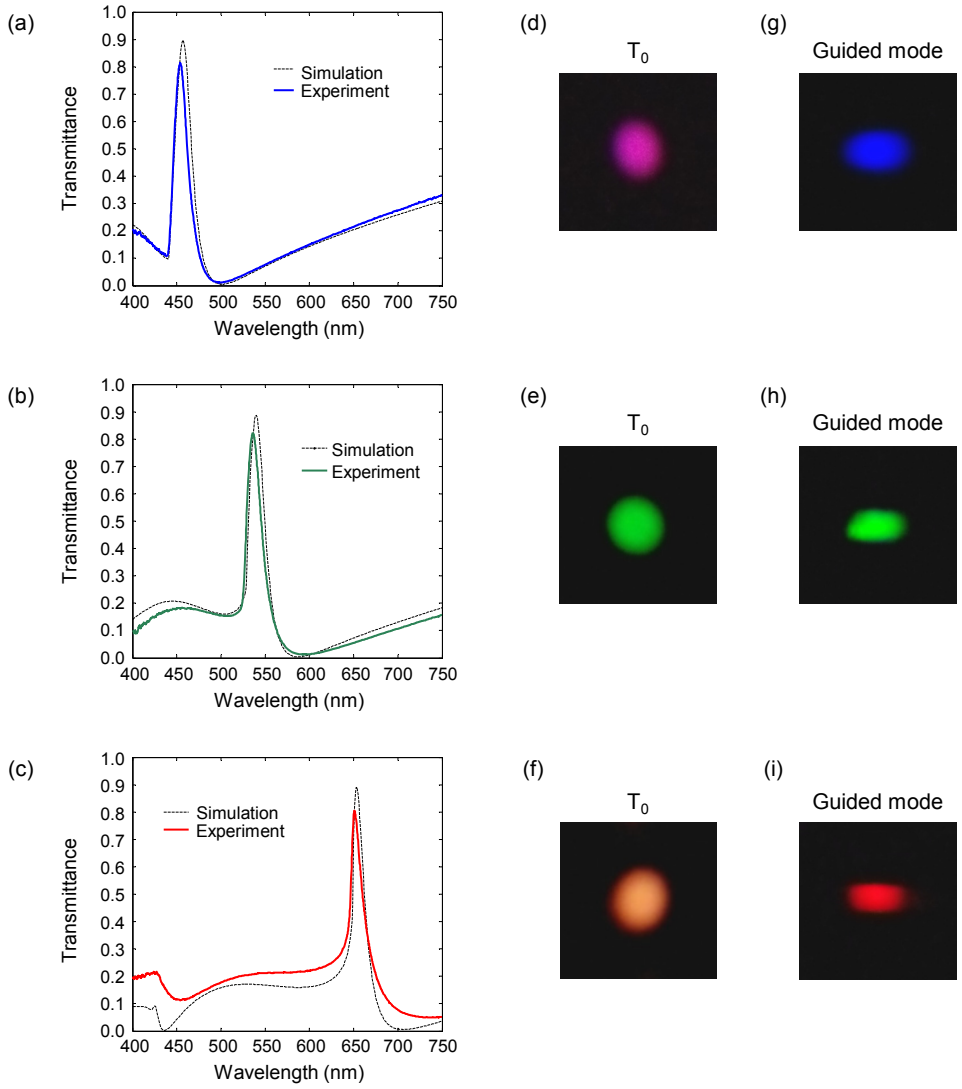

Fig. 6. Measured transmission spectra (solid curves) of fabricated (a) blue, (b) green, and (c) red filters in comparison with the simulated spectra (dashed curves); (d)–(f) show the color of the zero-order transmission and (g)–(i) show the color of the guided resonant modes of the filters.

Our fabricated devices show that it is possible to achieve high performance metallic transmission filters without any buffer cladding layer. The measured peak bandwidth (FWHM) of our devices is ~20 nm, which is significantly smaller than ~60 nm previously obtained with similar device architectures [14,15]. Since the transmission bandwidth depends on the index contrast between the waveguide and the substrate, other desired bandwidths may be obtained by using other available materials for the waveguide layer such as MgO (n_f ~1.7), Si_3N_4 (n_f ~2.0), and TiO_2 (n_f ~2.5). For color filters using metallic waveguide gratings, inclusion of a buffer cladding layer between the metal film and waveguide core may lead to further reduction of transmission bandwidth as Kaplan *et al.* showed in [15]. Table 1 summarizes all designed and measured parameters.

#223907 - $15.00 USD Received 26 Sep 2014; revised 19 Nov 2014; accepted 25 Nov 2014; published 4 Dec 2014

Table 1. Designed and measured parameters for the blue, green, and red filters

	Blue		Green		Red	
Parameters	Designed	Measured	Designed	Measured	Designed	Measured
Λ (nm)	290	291	350	349	430	428
F	0.670	0.656	0.670	0.665	0.670	0.678
t_g(nm)	40	40	40	40	40	38
t_f (nm)	200	203	200	203	200	208
$\lambda_{resonanc}$(nm)	456	454	541	536	655	651
FWHM (nm)	22	19	20	20	14	19

5. Conclusion

In summary, we design, fabricate, and test high-performance color filters grounded in coexisting GMR and SPR effects while being influenced by a nearby Rayleigh anomaly. In our design, an SPR at the interface between the Al grating and the Al_2O_3 film contributes to transmission suppression while a narrow transmission peak is formed by a GMR whose spectral shape is affected by a Rayleigh anomaly. We find that the narrow bandwidth obtained is, in large measure, due to the low index contrast between the waveguide film and the substrate. We experimentally achieve filter efficiency above 80% with narrow bandwidth of 20 nm in good agreement with the theoretical predictions. This excellent performance is obtained using a single waveguide layer without an additional buffer cladding layer separating the metal and waveguide core region. Images of the zero-order transmission spectra and side-coupled resonant output light confirm that this class of devices has promising applications in color filtering. Our results provide basis for further work to improve color purity by further suppressing sidebands and to optimize analogous 2D-grating devices working with unpolarized light.

Acknowledgments

This research was supported, in part, by the Texas Instruments Distinguished University Chair in Nanoelectronics endowment. D. B. Mazulquim was supported by the CAPES Foundation (11494/13-1).

#223907 - $15.00 USD Received 26 Sep 2014; revised 19 Nov 2014; accepted 25 Nov 2014; published 4 Dec 2014